

Muon Scattering Tomography for Non-Destructive testing of high Z materials: An experimental and a simulation study with Geant4

Ramkrishna Joshi

IIT Hyderabad

May 28, 2025

Contents Overview

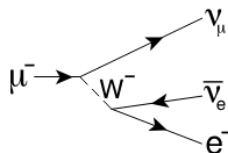
1. Introduction: What are muons and how they can be of our help?
2. Brief introduction to Muon Scattering Tomography
3. Workflow and Methodology
4. Experimental setup
5. Efficiency measurements of CAEN detection module
6. Experimental muon flux attenuation through concrete targets
7. Geant4 simulation setup
8. Study of no defect concrete and lead targets
9. Study of complete and partial defect lead targets
10. Summary and Conclusions
11. Future projects
12. References

Cosmic muons: Introduction

- Muons are fundamental subatomic particles, similar to electrons but heavier with $m_\mu \approx 207m_e$.
- Interacts via gravity, electromagnetic, and weak forces.
- Charge: $-1e$, Spin: $\frac{1}{2}\hbar$, Antiparticle: μ^+ , Lifetime: Approximately 2.2 microseconds.
- Decays into an electron, a muon neutrino, and an electron antineutrino (most common decay).
- Discovered in 1936 by Carl D. Anderson and Seth Neddermeyer.

Three generations of matter (fermions)

	I	II	III	
mass	2.4 MeV/c ²	1.27 GeV/c ²	173.2 GeV/c ²	0
charge	$\frac{2}{3}$	$\frac{2}{3}$	$\frac{2}{3}$	0
spin	$\frac{1}{2}$	$\frac{1}{2}$	$\frac{1}{2}$	1
name	u up	c charm	t top	γ photon
Quarks	4.8 MeV/c ² $-\frac{1}{3}$ d down	164 MeV/c ² $-\frac{1}{3}$ s strange	4.2 GeV/c ² $-\frac{1}{3}$ b bottom	0 0 1 g gluon
	< 2.2 eV/c ² 0 $\frac{1}{2}$ ν_e electron neutrino	< 0.17 MeV/c ² 0 $\frac{1}{2}$ ν_μ muon neutrino	< 15.5 MeV/c ² 0 $\frac{1}{2}$ ν_τ tau neutrino	91.2 GeV/c ² 0 0 1 Z ⁰ Z boson
	0.511 MeV/c ² -1 $\frac{1}{2}$ e electron	105.7 MeV/c ² -1 $\frac{1}{2}$ μ muon	1.777 GeV/c ² -1 $\frac{1}{2}$ τ tau	80.4 GeV/c ² ± 1 1 W ^{\pm} W boson
Leptons				Gauge bosons



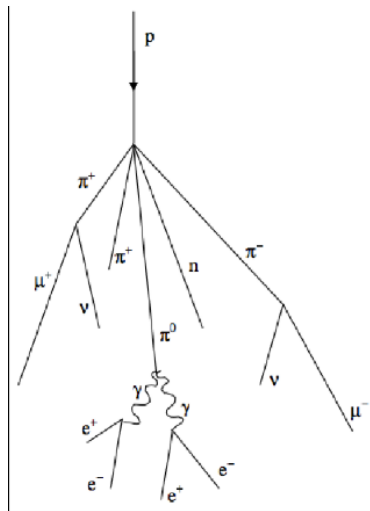
Cosmic Rays: High-Energy Radiation

Primary Cosmic Rays

- High-energy particles from outer space, mainly protons, continually bombard Earth.
- Energy range: 10^9 eV (1 GeV) to 10^{20} eV. Composition: 95% protons, 4% helium nuclei, 1% other elements.

Secondary Cosmic Rays

- Produced when primary cosmic rays interact with Earth's atmosphere.
- Cascade of particles includes pions, muons, electrons, and neutrinos. Muons are the most common secondary cosmic rays detected at Earth's surface.
- **Good estimate of flux of muons is $\approx 1 \text{ muon/minute.cm}^2$**



Muon Scattering Tomography (MST)

- **Muon Scattering Tomography (MST)** is a non-invasive imaging technique that utilizes cosmic ray muons to probe the internal structure of dense materials.
- It exploits the natural flux of high-energy muons from cosmic rays that can penetrate thick layers of matter.
- Detectors placed above and below the target track incoming and outgoing muon trajectories.
- Muon scattering angles provide information about the material's density and atomic number (Z).
- Applications:
 - Health monitoring of small civil structures
 - Nuclear waste imaging
 - Cargo inspection
 - Geophysical exploration

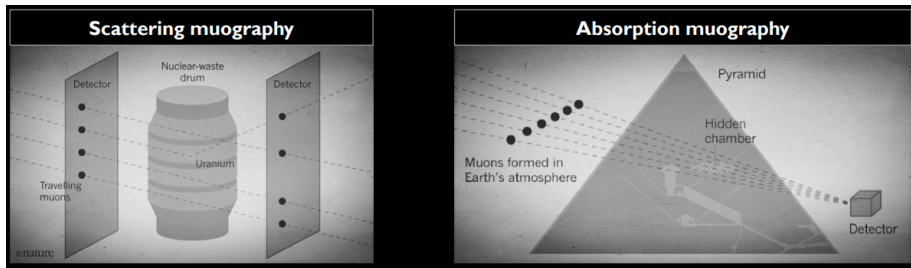


Figure: Applications of MAT and MST

source: M. Lagrange, Introduction to Muography, Working Experience Week, CERN Indico, 2024.

<https://indico.cern.ch/event/1395474/contributions/5865876/attachmen>

Role of Multiple Coulomb Scattering (MCS) in MST

- As muons pass through a material, they undergo **Multiple Coulomb Scattering (MCS)** due to interactions with atomic nuclei.
- The root-mean-square (RMS) scattering angle θ_0 is approximately (Wen, 2023):

$$\theta_0 = \frac{13.6 \text{ MeV}}{\beta p} z \sqrt{\frac{x}{X_0}} \left[1 + 0.038 \ln \left(\frac{x}{X_0} \right) \right]$$

where:

- p = muon momentum
- x = thickness of material
- X_0 = radiation length
- High- Z materials cause greater scattering—useful for discriminating materials.
- MST algorithms use ML models to reconstruct 3D images by analyzing scattering angles across many muon tracks.

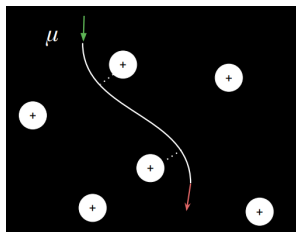


Figure: Path of muons through material

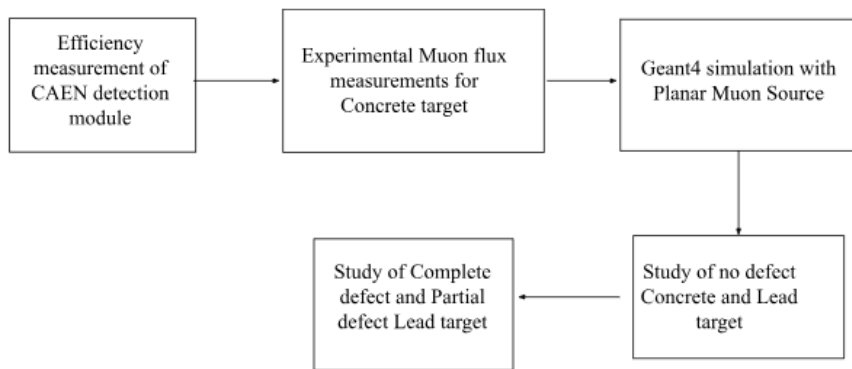
Scattering amplitude	Material density [g.cm^{-3}] (related to number of nuclei per unit of volume)	Atomic number Z (number of proton per nuclei)
Large	Large	Large
Medium	Large	Low
Medium	Low	Large
Low	Low	Low

Table: Scattering amplitude for varying material density and atomic number

source: M. Lagrange, Introduction to Muography, Working Experience Week, CERN Indico, 2024.

<https://indico.cern.ch/event/1395474/contributions/5865876/attachmen>

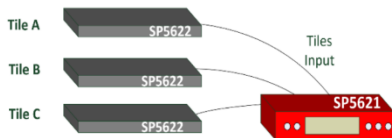
Workflow



- ① Assemble CAEN Cosmic Hunter system with 3 scintillator detectors and coincidence module. We take readings for triple and double coincidence modes.
- ② We measure the efficiency of each detector tile by taking ratio of triple coincidence and respective double coincidence readings.
- ③ This is followed by muon flux measurements for:
 - Without concrete blocks acting as obstruction (baseline).
 - With fiber-reinforced concrete blocks acting as obstruction (target under test).
- ④ We simulate the four detector and target geometry in Geant4 with concrete and lead blocks.
- ⑤ First experimental setup in Geant4 is for targets with no defects.
- ⑥ We introduce complete and partial hole defects in simulation targets and take muon flux measurements.
- ⑦ Final step is analyzing muon flux variation and scattering due to defect geometry.

Experimental setup

Determining Efficiency of Detector

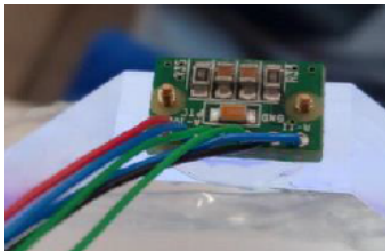


Concrete Slabs Experiment

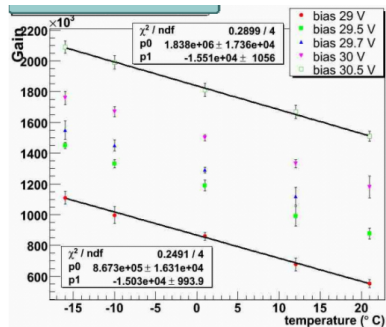


CAEN detection module

- The detection module consists of plastic scintillators coupled to SiPMs.
- Detection efficiency of SiPM varies with temperature due to changing overvoltage.
- Thus characterizing the CAEN detector and calculating efficiencies is an important task.,



(a) SiPM coupled to plastic scintillator



(b) Gain of SiPM as a function of temperature

Framework for determining the efficiency of tiles

- In the experiment, three detectors named A,B and C; are stacked on top of each other. Thus for the triple coincidence, the number of detected muons in P^{th} detection cycle is given by;

$$N_P^3 = N_0 \epsilon_i \epsilon_j \epsilon_k$$

Where N_0 is the initial number of muons reaching the topmost detector and N_P^3 is the number of muons detected after triple coincidence. $\epsilon_i/j/k$ represents the detection efficiency of $i^{th}/j^{th}/k^{th}$ detector.

- In order to develop a model independent of N_0 , we also measure double coincidence with ij, ik and jk detectors. For double coincidence with detectors i and j, number of detected muons in P^{th} cycle is given by;

$$N_P^2 = N_0 \epsilon_i \epsilon_j$$

- Thus a general procedure for determining the efficiency of k^{th} detector is;

$$N_P^3 / N_P^2 = N_0 \epsilon_i \epsilon_j \epsilon_k / N_0 \epsilon_i \epsilon_j$$

ABC coincidence: Binned temperature dependence

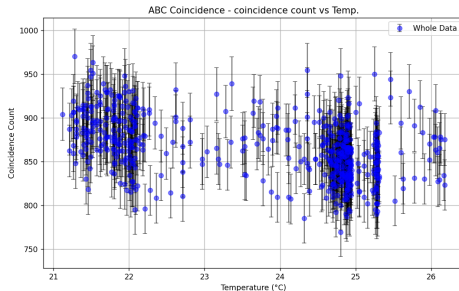


Figure: ABC coincidence variation with temperature

- The data represents the variation of triple and double coincidence cosmic muon count with temperature over 586 cycles of 10 minutes each. Error in detected muon count for P^{th} detection cycle is $\sqrt{N_P^3}$.
- Two prominent clusters can be identified in the plot, namely the $21^0C - 22^0C$ cluster and the $24^0C - 25^0C$ cluster.

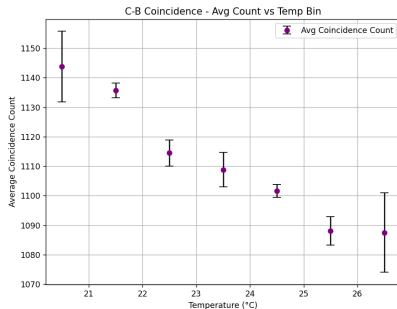
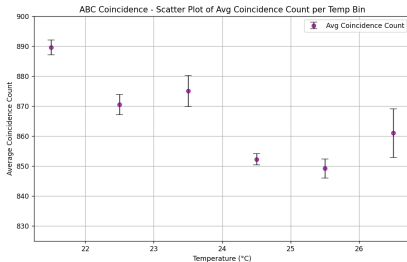


Figure: Scatter plot showing variation of average ABC coincidence count (left) and average CB coincidence count (right) with temperature.

- Overall trend suggests that the coincidence count reduces at higher temperatures.

Efficiency of tile A

- The efficiency of tile A now can be readily calculated by calculating, $\epsilon_A = N(ABC, T)/N(CB, T)$

Temp Bin(C^0)	Avg ABC Count	Avg CB Count	ϵ_A	$\delta\epsilon_A$
21-22	889.65 ± 2.47	1135.70 ± 2.54	0.783	0.002
22-23	870.49 ± 3.36	1114.45 ± 4.46	0.781	0.004
23-24	875.07 ± 5.15	1108.82 ± 5.80	0.789	0.007
24-25	852.27 ± 1.90	1101.62 ± 2.12	0.774	0.002
25-26	849.17 ± 3.22	1088.11 ± 4.81	0.781	0.004

Table: Table of Avg ABC and CB coincidence counts, calculated ϵ_A , and its error.

- This method can be used to calculate efficiency of detector tiles B and C as well.

A-C coincidence binned temp data

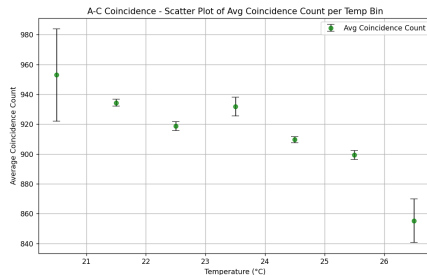
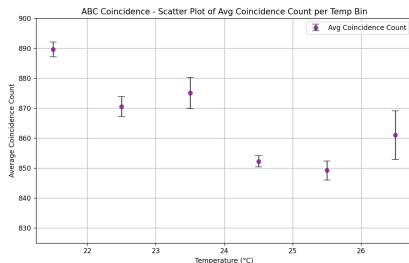


Figure: Scatter plot showing variation of average ABC coincidence count (left) and average AC coincidence count (right) with temperature.

- Overall trend suggests that the coincidence count reduces at higher temperatures.

Efficiency of tile B

- The efficiency of tile A now can be readily calculated by calculating, $\epsilon_B = N(ABC, T)/N(AC, T)$

Temp Bin($^{\circ}\text{C}$)	Avg ABC Count	Avg AC Count	ϵ_B	$\delta\epsilon_B$
21–22	889.650 ± 2.470	934.360 ± 2.290	0.952	0.004
22–23	870.490 ± 3.360	918.650 ± 3.030	0.948	0.005
23–24	875.070 ± 5.150	931.870 ± 6.370	0.939	0.009
24–25	852.270 ± 1.900	909.600 ± 2.110	0.937	0.003
25–26	849.170 ± 3.220	899.400 ± 2.990	0.944	0.005

Table: Table of Avg ABC and AC coincidence counts, calculated ϵ_B , and its error.

A-B coincidence binned temp data

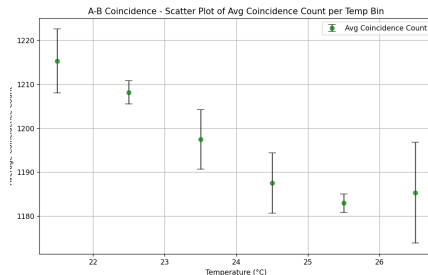
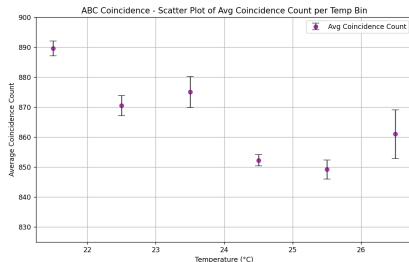


Figure: Scatter plot showing variation of average ABC coincidence count (left) and average AB coincidence count (right) with temperature.

- Overall trend suggests that the coincidence count reduces at higher temperatures.

Efficiency of tile C

- The efficiency of tile A now can be readily calculated by calculating,
 $\epsilon_C = N(ABC, T)/N(AB, T)$

Temperature (°C)	ABC Count	AB Count	ϵ_C	$\delta\epsilon_C$
21–22	889.65 ± 2.47	1215.30 ± 7.27	0.732	0.005
22–23	870.49 ± 3.36	1208.16 ± 2.64	0.721	0.003
23–24	875.07 ± 5.15	1197.46 ± 6.79	0.731	0.006
24–25	852.27 ± 1.90	1187.52 ± 6.89	0.718	0.004
25–26	849.17 ± 3.22	1182.94 ± 2.10	0.718	0.003

Table: Efficiency of Tile C (ϵ_C) and its uncertainty across temperature bins.

Summary of tile efficiencies

Temp Bin ($^{\circ}\text{C}$)	$\epsilon_A \pm \delta\epsilon_A$	$\epsilon_B \pm \delta\epsilon_B$	$\epsilon_C \pm \delta\epsilon_C$
21–22	0.783 ± 0.002	0.952 ± 0.004	0.732 ± 0.005
22–23	0.781 ± 0.004	0.948 ± 0.005	0.721 ± 0.003
23–24	0.789 ± 0.007	0.939 ± 0.009	0.731 ± 0.006
24–25	0.774 ± 0.002	0.937 ± 0.003	0.718 ± 0.004
25–26	0.781 ± 0.004	0.944 ± 0.005	0.718 ± 0.003

Table: Efficiencies ϵ_A , ϵ_B , and ϵ_C with associated errors across different temperature bins.

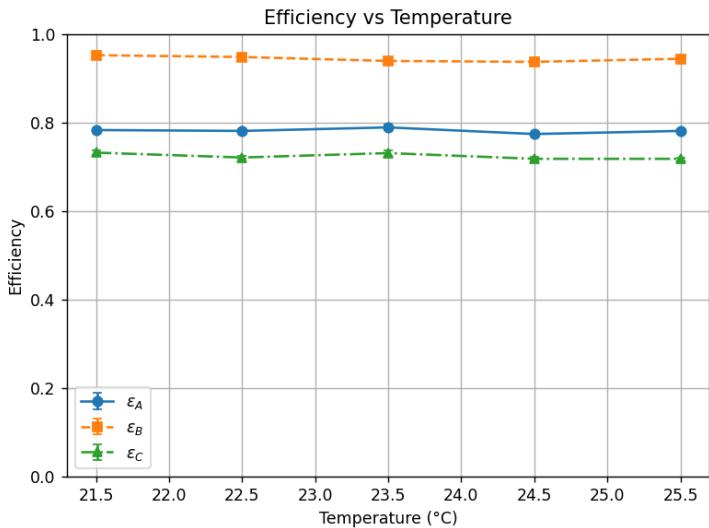


Figure: Comparison of efficiencies of all tiles plotted against temp bins

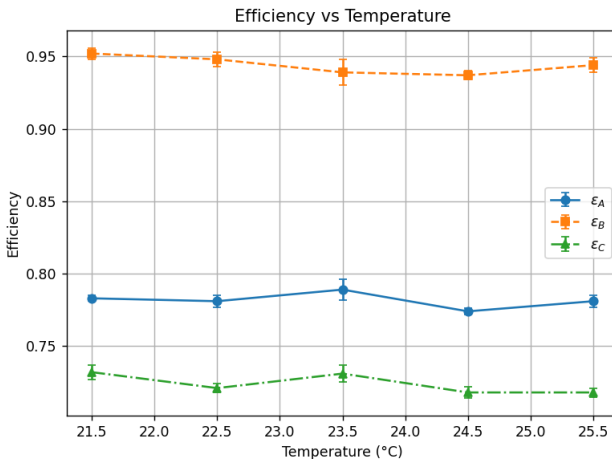


Figure: Comparison of efficiencies of all tiles plotted against temp bins with changed y axis limits

Experimental Setup



Figure: Comparison of experimental setups with and without concrete slabs.

Concrete slabs experiment Run 1

- In this experiment, we place concrete slabs between detector A and detectors BC to determine flux attenuation of muons as they pass through the concrete slab. We record ABC coincidence over a range of temperature to determine the attenuation effect. For this experiment we have performed three runs. Run 1 lasted for 889 detection cycles.

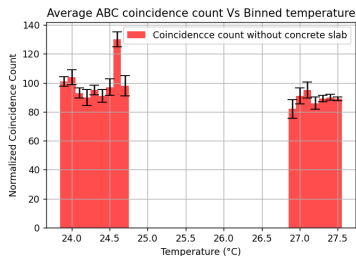
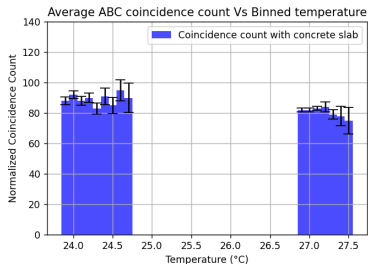


Figure: Comparison of average ABC coincidence count with and without a concrete slab for different binned temperatures.

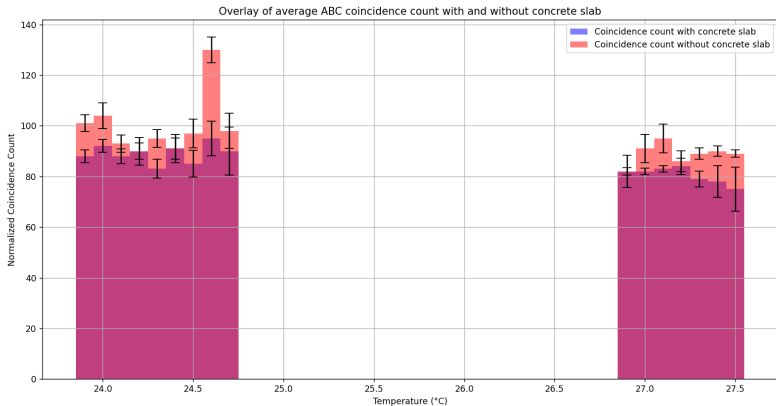


Figure: Plot shows the comparison between the average ABC coincidence count when the concrete slab was placed and when no slab was placed. Comparison is presented across multiple temperature bins with $0.10\text{ }^{\circ}\text{C}$ width.

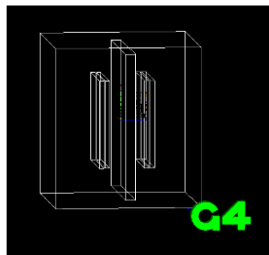
- It can be observed that across different temperature bins, the coincidence count was smaller when the concrete slab was placed.

Concrete Slabs Experiment: Run 2

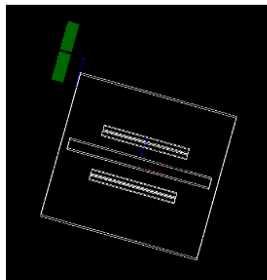
- We repeated the experiment in trial run 2, which lasted for 2 hours.
- The data consists of 1 hour of readings without a concrete slab and 1 hour of readings with a concrete slab.
- ABC coincidence count:
 - Without concrete slab: 561 ± 24
 - With concrete slab: 462 ± 21

Geant4 simulation setup and geometry

- Geant4 simulation geometry consists of four detectors (two before target and two after it), one target, and a planar source of muons.
- Target dimensions are $1.0m \times 1.0m$ with varying thickness. Source dimensions are $0.6m \times 0.6m$. Detector dimensions are of $0.6m \times 0.6m \times 0.03m$.



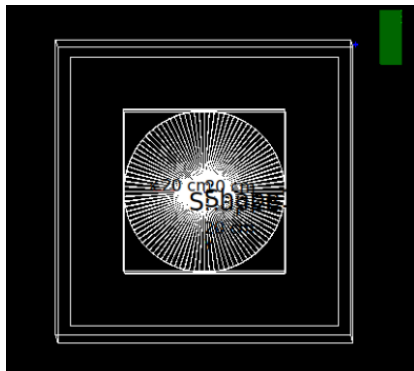
(a)



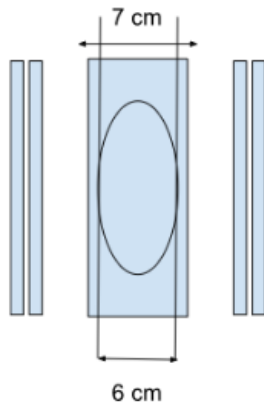
(b)

Figure: Experimental geometry in Geant4 simulation setup

Complete and Partial hole defects



(a) Complete hole defect



(b) Partial hole defect

Figure: Schematics of target configurations: (a) with complete circular defect and (b) with partial circular hole defect of thickness 6 cm.

Concrete target with varying thickness

- For concrete targets we study the muon count recorded at the two bottom detectors B1 and B2.
- We vary the thickness of the target to understand the trend in the muon flux attenuation as a function of the target thickness.
- We consider thickness of 10 cm, 15 cm, 18.8 cm (same as experimental setup concrete thickness) and 25 cm.

Table: Muon counts for concrete slab without hole (100,000 muons run)

Slab Thickness (cm)	B1	B2	T2	T1
10	96969	96410	99987	99933
15	96313	95596	99989	99924
18.8	96097	95239	99990	99933
25	95172	94133	99985	99925

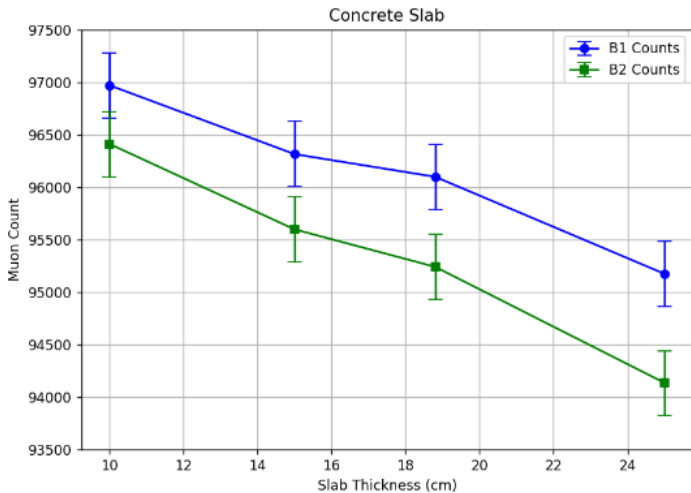
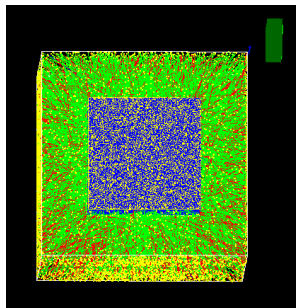
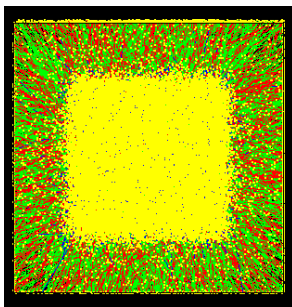


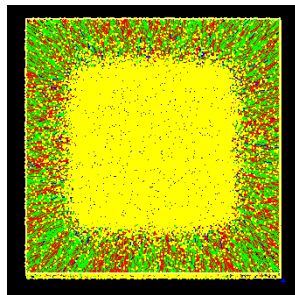
Figure: B1 and B2 detector counts for concrete slab with varying thickness



(a) Source pattern



(b) 10 cm concrete



(c) 18.3 cm concrete

Figure: Comparison of (a) the original source pattern, (b) scattering after 10 cm of concrete, and (c) scattering after 18.3 cm of concrete.

Lead target with varying thickness

- For lead target, by following the similar procedure, we vary the thickness of the target and record muon counts.
- There is significantly more scattering observed for the lead target.
- Muon counts at B1 and B2 detectors are significantly lesser for lead target as compared to concrete target.

Table: Muon count for Lead slab without hole (100,000 muons run)

Slab Thickness (cm)	B1	B2	T2	T1
5	90145	87940	99983	99938
7	86895	84089	99985	99952
9	82124	77958	99991	99940
11	75689	71564	99989	99925

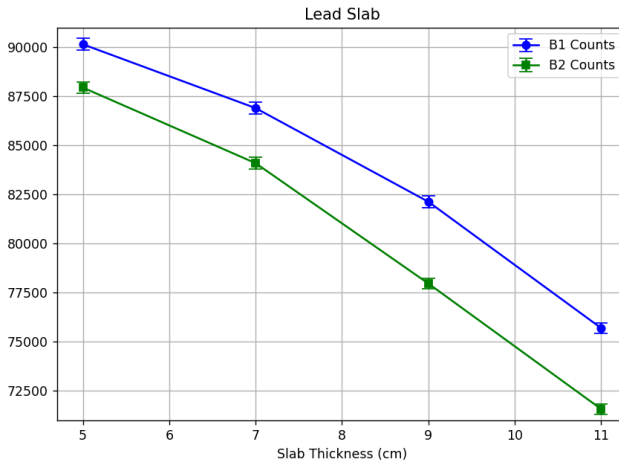
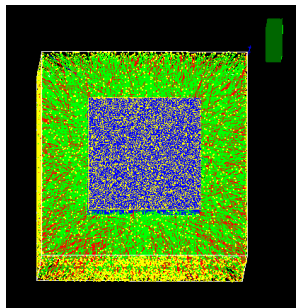
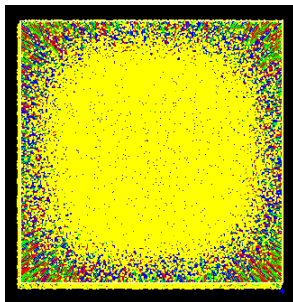


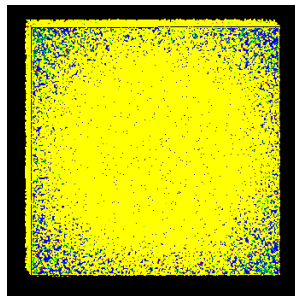
Figure: B1 and B2 detector counts for lead slab with varying thickness



(a) Source pattern



(b) 5 cm lead



(c) 9 cm lead

Figure: Comparison of (a) the original source pattern, (b) scattering after 5 cm of lead, and (c) scattering after 9 cm of lead.

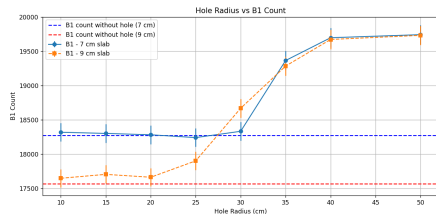
Lead target with complete hole defect

- Lead slab of thickness 7 cm and 9 cm is considered. We vary the radius of the circular defect from 10 cm to 50 cm considering 9 different radii.

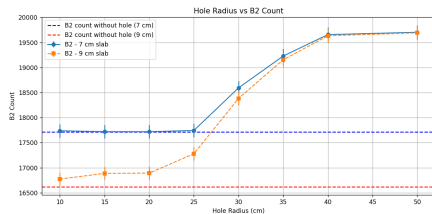
Lead slab thickness: 7 cm					Lead slab thickness: 9 cm				
Hole radius	B1	B2	T2	T1	Hole radius	B1	B2	T2	T1
10 cm	18320	17737	20000	19993	10 cm	17649	16773	19998	19987
15 cm	18303	17720	19993	19985	15 cm	17706	16887	19998	19998
20 cm	18283	17719	19993	19989	20 cm	17664	16893	19999	19987
25 cm	18242	17743	19997	19988	25 cm	17903	17278	19990	19982
30 cm	18834	18594	19993	19977	30 cm	18670	18384	19996	19987
35 cm	19366	19229	19999	19983	35 cm	19285	19156	19997	19979
40 cm	19698	19656	19999	19986	40 cm	19673	19633	19997	19984
50 cm	19743	19703	19995	19991	50 cm	19733	19692	19996	19991

- Clear trend is observed in increasing muon count with increasing hole radius. This shows that MST has a definite application in detecting defect in target material.

Plots and scattering patterns for complete hole defect

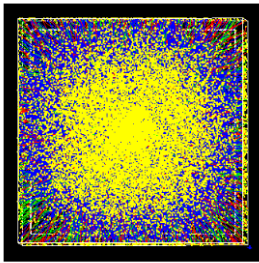


(a)

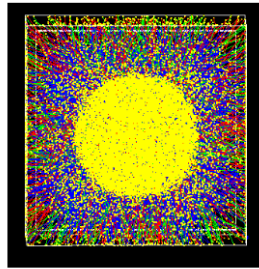


(b)

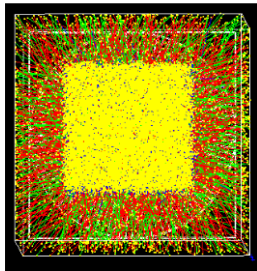
Figure: Muon counts at B1, panel (a) and B2, panel (b) detectors. Dotted lines are reference points with MST readings for no defect targets.



(a)



(b)



(c)

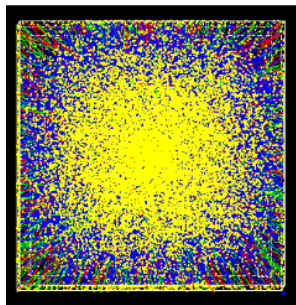
Figure: Comparison of scattering patterns as observed on the screen for lead slab of 7 cm with central hole radius (a) 10 cm, (b) 30 cm, and (c) 50 cm.

Lead target with partial hole defect

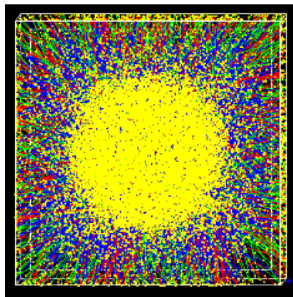
- Lead slab of thickness 7 cm is considered. We vary the radius of the circular defect from 10 cm to 50 cm considering 9 different radii.
- Partial hole thickness of 6 cm and 5 cm is considered for simulation.

Slab Thickness	Hole Radius	B1	B2	T2	T1
7 cm	10 cm	18303	17689	19993	19978
	15 cm	18252	17663	19994	19983
	20 cm	18285	17734	19993	19983
	25 cm	18325	17863	19999	19982
	30 cm	18749	18491	19999	19990
	35 cm	19159	18953	19995	19982
	40 cm	19320	19146	20000	19992
	50 cm	19422	19250	19999	19989

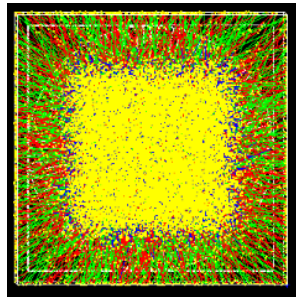
Figure: Muon counts for 7 cm lead slab thickness with 6 cm hole thickness across varying hole radii.



(a)



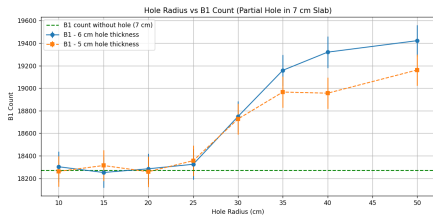
(b)



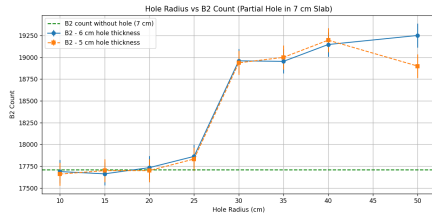
(c)

Figure: Muon scattering pattern for a lead block with partial holes of radii (a) 10 cm, (b) 30 cm, and (c) 50 cm for hole thickness of 6 cm

Plots for partial hole defect



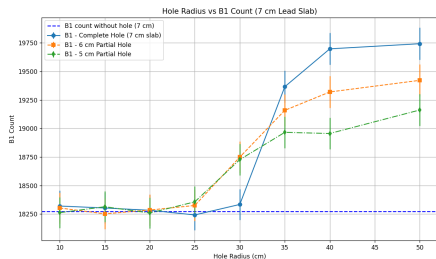
(a)



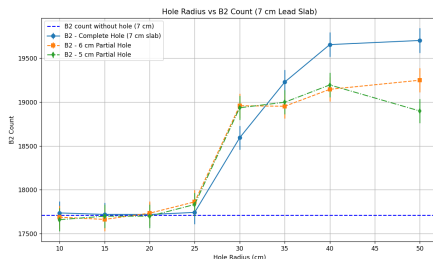
(b)

Figure: Plots show muon counts with varying partial hole defect radius for 6 cm and 5 cm thick defects in a 7 cm thick lead slab for B1 and B2 detectors.

Comparison plots for all three cases



(a)



(b)

Figure: Plot shows combined results for muon counts at B1 detector (panel a) and B2 detector (panel b) for the no defect, complete defect and partial defect lead slab cases.

Summary and conclusions

- Two experiments were performed namely, determining the detection efficiency and studying the attenuation effects of concrete slab on muon flux
- Detector B had the highest detection efficiency. Detection efficiency of A and C are close by and lesser than B.
- In both trial runs, notable attenuation in the ABC coincidence count was observed when the concrete slab was placed between detector A and detectors B,C.
- Reduction in the coincidence count was seen with increasing thickness for concrete as well as lead target in the Geant4 setup.
- We have successfully confirmed unique scattering patterns with a planar muon source for complete and partial defects of different sizes and dimensions. These scattering patterns can aid the identification of the defect to map the internal volume of the target.
- Geant4 simulation confirms that the highest degree of attenuation and MCS is observed for no defect targets followed by partial defect and complete defect targets.

Future prospects and Acknowledgment

- This study marks the preliminary understanding of the experimental and simulation based MST and MAT.
- Future work will involve integrating high efficiency pixelate detectors in the experimental setup to accurately map out the scattering pattern and study scattering amplitudes.
- Future simulation work will involve using CRY cosmic muon library for mimicking the angular spectrum of muons before their interaction with the target. This step would likely involve more computational complexity and increased computation time.

We would like to sincerely thank the Civil Engineering Department at IIT Hyderabad for providing us concrete targets which have been very useful in our experimentation.

References I



M. Lagrange, *Introduction to Muography*, Working Experience Week, CERN Indico, 2024.
<https://indico.cern.ch/event/1395474/contributions/5865876/attachments>



CMS Collaboration, *Muon Tomography*, CMS Experiment, CERN, 2024. <https://cms.cern/content/muon-tomography>.



Qun-Gang Wen, *Research on rapid imaging with cosmic ray muon scattering tomography*, Scientific Reports, vol. 13, Article number: 19718, 2023. <https://doi.org/10.1038/s41598-023-47023-w>.







L. Bonechi, R. D'Alessandro, and A. Giammanco, *Atmospheric muons as an imaging tool*, Reviews in Physics, vol. 5, 100038, 2020.



P. Stowell *et al.*, *Figures of Merit for the Application of Muon Tomography to the Characterization of Nuclear Waste Drums-19253*, WM2019 Conference, Phoenix, Arizona, 2019.

References II

-  C. Thomay *et al.*, *Passive 3D imaging of nuclear waste containers with Muon Scattering Tomography*, Journal of Instrumentation, vol. 11, P03008, 2016.
-  S. Pesente *et al.*, *First results on material identification and imaging with a large-volume muon tomography prototype*, Nuclear Instruments and Methods in Physics Research A, vol. 604, pp. 738–746, 2009.
-  M. Stapleton *et al.*, *Angle Statistics Reconstruction: a robust reconstruction algorithm for Muon Scattering Tomography*, Journal of Instrumentation, vol. 9, P11019, 2014.
-  K. N. Borozdin *et al.*, *Image reconstruction and material Z discrimination via cosmic ray muon radiography*, Nuclear Instruments and Methods in Physics Research A, vol. 513, pp. 554–558, 2003.

Thank You!

I appreciate your time and attention.